PEM electrolysis: Degradation study of N1110 assemblies for the production of green hydrogen

G. Tejera[1], R. Rojas[1], E. Teliz[1,2], V. Diaz[1]
[1]GIIE, Facultad de Ingeniería, UdelaR, J. Herrera y Reissig 565, CP 11300, Montevideo, Uruguay.
[2]GIIE,Facultad de Ciencias, UdelaR, Iguá 4225, CP 11400, Montevideo, Uruguay
e-mail: verodiaz@fing.edu.uy

Abstract

The production of hydrogen through proton exchange membrane water electrolysis (PEMWE) is seen as a key solution for sustainable energy generation. However, the durability and stability of Proton Exchange Membrane (PEM) cells components, particularly Membrane-Electrode Assemblies (MEAs), remain crucial challenges to overcome for scalability. In this study, the degradation of a 25 cm^2 CCM-type MEA was systematically investigated, using N1110 as the polymeric electrolyte and an anodic and cathodic loading of 3mg/cm^2 of PtB. A PEM electrolysis test bench was subjected to controlled operating conditions corresponding to 2V and 60°C for two stages of 168 hours each, conducting a detailed analysis of performance behavior before, during, and after each degradation period. Electrochemical techniques were employed to characterize the performance stability: chronoamperometry, linear polarization curves, and electrochemical impedance spectroscopy (EIS). The EIS experimental results were fitted to equivalent electrical circuits and the parameters corresponding to ohmic resistances, charge transfer, and diffusional processes were determined. An increase in the resulting time constants and ohmic resistance was depicted because of the degradation.
After a straightforward treatment rinsing the assembly with a 1 mol/L H_2SO_4 solution, the MEA partially regained its initial performance, depicting a degradation rate six times slower than one observed before regeneration in acidic media. This point suggests that the temporary decline in performance of the MEA is primarily due to reversible contamination.

Keywords: PEM electrolyzer, hydrogen, degradation, membrane electrode assemblies, electrolysis, electrochemical impedance spectroscopy, voltammetry, PEMWE.

1. Introduction

In recent years, significant attention has been directed towards PEMWE within scientific circles. This surge in interest stems partly from the imperative to transition towards cleaner energy sources, mitigating harmful emissions [1, 2].
Despite their pivotal role in facilitating the energy transition and the pursuit of climate neutrality, PEM electrolyzers still grapple with a range of challenges hindering their widespread adoption. While they offer the promising prospect of decentralized energy production and storage from renewable sources, several hurdles must be surmounted to unlock their full potential and make them economically viable on a large scale. Although production capacity has increased, which led to a significant reduction in prices, commercial costs remain elevated, primarily due to the utilization of precious metals. Thus, cost remains a formidable barrier to their broad commercialization.

Furthermore, ensuring the durability of electrolyzers is another critical obstacle to overcome for their widespread commercial adoption. Despite claims by many commercial PEM electrolyzer manufacturers regarding durability, boasting operational lifespans of up to 50,000 hours or even more, achieving consistent performance over extended periods remains a key challenge that needs to be addressed.

As commercial electrolyzer manufacturers strive to reduce costs and enhance performance, it's increasingly likely that durability will assume even greater importance. This trend may see manufacturers opting for reduced catalyst loading or alternative catalysts, as well as thinner or alternative membranes. Over time, PEM electrolyzers can degrade or experience an increase in operating voltage due to repetitive load cycles. While monitoring operating voltage can provide insights into overall device degradation, it fails to pinpoint specific degradation processes.

When it comes to the stability and durability of the electrocatalyst layer, there are several factors to consider. These include catalyst dissolution, surface blocking by external metal ions, catalyst agglomeration, and support passivation and corrosion [3, 4]

These issues can lead to a loss of contact between the catalyst and the electrode, a decrease in the thickness of the catalyst layer, and changes to the interface between the catalyst layer and membrane. This can result in a reduction of the electrochemically active surface area, leading to an increase in activation overpotential and electrical contact resistance.

PEMWE technology faces significant challenges on its path towards large-scale commercial viability. Research is focused on overcoming hurdles such as reducing the costs of catalysts, membranes, current collectors and bipolar plates, as well as improving manufacturing and assembly processes. Durability is a major concern, aiming for up to 100,000 hours of operation with minimal efficiency losses. Factors like the acidic environment, oxidation potential, and operational conditions impact component degradation. Recent studies have provided detailed analyses of these issues and suggested strategies to mitigate degradation and advance PEMWE development, aiming to position it as a key solution in the future of renewable energy.[7]

Bipolar plates (BPs) and gas diffusion layers serve multiple functions in PEMWE, including facilitating charge carrier transport between cells, supplying and removing reactants (such as water) and gases produced by the cell (such as H_2 and O_2), and maintaining the mechanical stability and integrity of the device. They also play a role in mass transport and heat management. These functions must be sustained in the high-pressure, oxidizing (at the anode) and reducing (at the cathode) conditions of electrolyzer operation throughout the system's lifespan (typically over 40,000 hours). BPs are crucial components in the PEMWE stack, accounting for 48% of the stack cost.[8, 9, 10]

The degradation of bipolar plates is primarily caused by corrosion, passivation, and hydrogen embrittlement. Due to the stringent requirements for corrosion and oxidation resistance at the anode, where high overpotentials (1.6-2.0 V) and low pH (2-4) electrolyte media are present, there are limited material options available for PEMWE.

Current collector degradation can generally be classified into chemical and mechanical degradation. Current collectors, serving as an interface between the MEA and BPs at both electrodes, transport liquid/gas two-phase fluid, conduct electrons with low resistance, and provide mechanical support for MEAs [11,12]

Current collectors are typically made of carbon or metal materials, with metallic materials preferred for the anode due to carbon's high corrosion rate in oxidative environments.[13],[14]

The pore size and structure of the current collector significantly impact fluid transport, with gas starvation or saturation leading to obstruction of reactant and product diffusion pathways, ultimately reducing device performance [15]

While the durability and degradation of current collectors are not extensively reported, their critical role in PEMWE cells is emphasized.

Compared to other components of PEMWE, the membrane is often considered the weakest component regarding long-term performance. Research on the durability and degradation of membranes in PEMWE is limited. Generally, membrane degradation can be classified into three main types: mechanical, thermal, and chemical/electrochemical.

Even though reactive intermediates produced in the MEA of PEMWE are effectively diluted as the electrolyzer is submerged in water, the decline in performance and durability of the membrane is typically due to pollution or chemical degradation [5, 6].

The constant hydration of membranes can cause swelling, also reducing the mechanical strength and integrity of the membrane.

Despite an increasing focus on PEM electrolyzer durability in research papers, several aspects remain relatively unknown or ambiguous, particularly concerning degradation testing procedures and result interpretation.

To discern different degradation processes, various electrochemical diagnostic methods are employed. In-situ testing methods such as linear polarization, EIS, and cyclic voltammetry (CV) are commonly utilized.

Complementary ex-situ methods like scanning electron microscopy (SEM), transmission electron microscopy (TEM), and X-ray crystallography (XRD) offer additional insights into localized system changes caused by degradation.

Stability tests or long-term tests, whose results are influenced by its time duration, temperature conditions, and operating conditions; provide a direct and practical methodology that helps to gain knowledge about the fundamental degradation processes of PEM membranes.[16]

This study presents stability tests, under potentiostatic and galvanostatic steps. The studied MEA was then subjected to a regeneration treatment.

2. Experimental

The electrochemical assessment of the studied PEM membrane electrode assemblies was conducted using a custom-built experimental electrolysis test bench. This test bench included a single-cell electrolyzer with a 25 cm^2 active area, a power supply, a peristaltic pump, a temperature controller, and rotameters. The test bench was supplied with demineralized water and electrical energy from the power supply.

The system temperature was managed by a NOVUS N1050 proportional, integral, and derivative (PID) process controller. Thermal energy was provided by two 60W heaters attached to the anodic and cathodic plates, operating at 120V. The temperature was set to 60°C (±0.2°C) and monitored by a Pt100 platinum sensor connected to the controller. The heaters raised the equipment temperature to the set point, after which the controller stopped the heat supply until a temperature drop was detected, ensuring it remained above the lower limit. The controller does not have a cooling function; it only halts the heat supply until the environment cools to the desired temperature. Cooling was not considered necessary because the

water supply was not heated, and the thermal dissipation between the electrolyzer, water reservoir, and environment was sufficient to cool the system when needed.

For this study, the assembly involves catalyst-coated membrane (CCM)- type with a geometric area of 25 cm^2 containing Nafion™ 1110, and 3.0 $mg.cm^{-2}$ PtB both for the anode and cathode catalyst. Sintered Ti plates were used as gas diffusion layers. CCM characterization is shown in Table 2.1.

Table 2.1. Catalyst coated membrane characterization

Membrane Type	PSFA Nafion™ N1110
Typical thickness (µm)	254
Membrane weight (g/m2)	500
Anodic catalyst	Platinium black
Anodic loading (mg/cm2)	3.0
Cathodic catalyst	Platinium black
Cathodic loading (mg/cm2)	3.0

The test bench was connected to a potentiostat galvanostat GAMRY© for electrochemical experiments. The final layout of the test bench is illustrated in Figure 2.1.

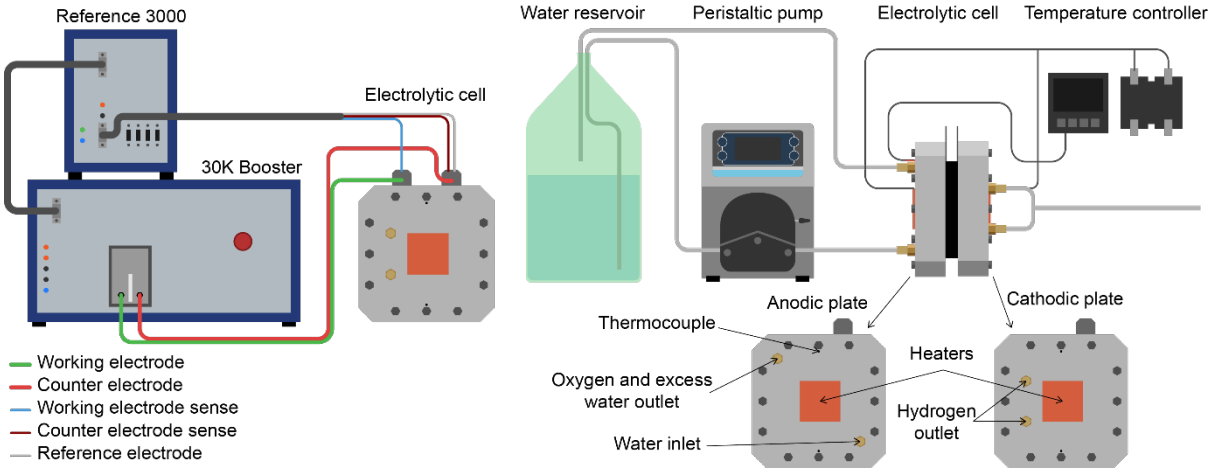

Figure 2.1 – Test bench diagram.

Before each test, activation of the membrane procedure was carried out, following the method reported in previous studies[17]. The cyclic voltammograms are presented in Figure 2.2.

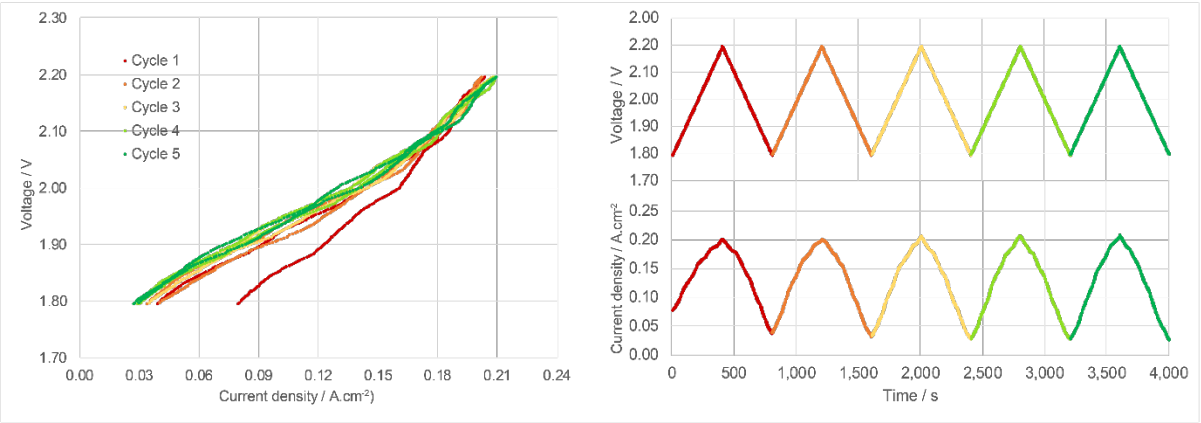

Figure 2.2 – Cell activation routine.

Likewise, at the start of each stage, electrochemical characterization was carried out. Linear voltammetry and EIS were performed, which allowed the initial state of the membrane to be recorded.

Additionally, a degradation mitigation procedure was tested, which consisted of a treatment with 1M H_2SO_4 after the three degradation phases, based on the works of Wei et al.[18], who carried out a similar process as a pretreatment of the MEA.

For the development of this study, a PEM electrolysis system was subjected to the steps listed in Table 2.2, with materials and stages detailed below.

Table 2.2 – Experimental procedure listed by stages: Stage 0 corresponds to the initial condition, Stages 1, 2, 3, and 5 correspond to the stages in which the membrane-electrode assembly (MEA) is degraded, and Stage 4 corresponds to the stage where the MEA is regenerated.

Stage	Step No.	Description	Conditions
0	1	Activation	5 cycles from 1.8V to 2.2V
	2	Polarization Curve	Sweep at 0.1mV/s from 1.5V to 2.5V
	3	Stabilization and EIS	EIS from 100mHz to 100kHz
1	4	Degradation	Constant potential of 2V, 168 h
	5	Activation	5 cycles from 1.8V to 2.2V
	6	Polarization Curve	Sweep at 0.1mV/s from 1.5V to 2.5V
	7	Stabilization and EIS	EIS from 100mHz to 100kHz
2	8	Degradation	Constant potential of 2V, 168 h
	9	Activation	5 cycles from 1.8V to 2.2V
	10	Polarization Curve	Sweep at 0.1mV/s from 1.5V to 2.5V
	11	Stabilization and EIS	EIS from 100mHz to 100kHz
3	12	Degradation	Constant current of 0.092 $A \cdot cm^{-2}$, 168 h
	13	Activation	5 cycles from 1.8V to 2.2V
	14	Polarization Curve	Sweep at 0.1mV/s from 1.5V to 2.5V
	15	Stabilization and EIS	EIS from 100mHz to 100kHz
4	16	Regeneration	Constant potential of 2V
	17	Activation	5 cycles from 1.8V to 2.2V
	18	Polarization Curve	Sweep at 0.1mV/s from 1.5V to 2.5V
	19	Stabilization and EIS	EIS from 100mHz to 100kHz
5	20	Degradation	Constant potential of 2V, 168 h
	21	Activation	5 cycles from 1.8V to 2.2V
	22	Polarization Curve	Sweep at 0.1mV/s from 1.5V to 2.5V
	23	Stabilization and EIS	EIS from 100mHz to 100kHz

Electrochemical Impedance Spectroscopy (EIS)

EIS measurements were performed at different points of the polarization curve, sweeping a frequency range between 100 kHz and 10 mHz, with an amplitude of 5 mV and taking 10 points per decade. EIS experimental values for 1.9 V and 2.3 V were truncated only to include the ones with negative reactive impedance and fitted to the equivalent electrical circuit model depicted in Figure 2.3.

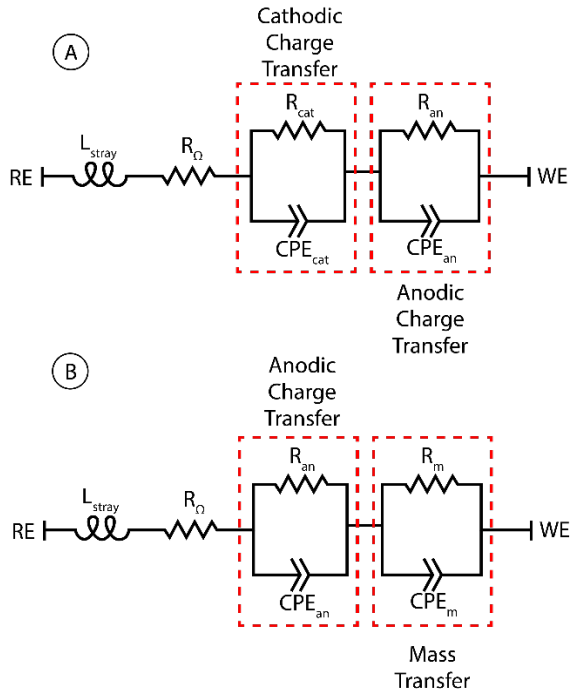

Figure 2.3 – Electrical circuit models where A was used to fit 1.9V data and B was used to fit 2.3V data.

The electrical circuits were selected once the corresponding Nyquist diagrams were obtained, to implement the least number of components, thereby reducing the number of parameters and the model complexity as much as possible. Although both equivalent circuits consist of the same components, their physical interpretations differ. On the one hand, Circuit A shown in Figure 2.3, was chosen for cases where only charge transfer phenomena are observed, which is the case for all EIS measurements at 1.9 V. On the other hand, Circuit B is used for measurements taken at 2.3 V, where mass transfer effects are evident. RE and WE correspond to the reference and working electrode respectively. L_{stray} models the inductance of the system while R_Ω, R_{cat}, R_{an} and R_m represent the ohmic, cathodic charge transfer resistance, anodic charge transfer resistance and mass transfer resistance respectively. CPE_{cat}, CPE_{an} and CPE_m denote the constant phase elements for the cathodic, anodic and mass transfer components respectively.

Degradation procedure

The degradation protocol consists of a total of 5 stages with different operational conditions: For stages 1 and 2, the electrolizer is operated in a potentiostatic manner. A potential of 2 V was maintained for a week (168 hours), which was sufficient to observe the degradation phenomenon. Stage 3 involves chronopotentiostatic degradation carried out at a constant current density of 0.08 A·cm^-2 for a week. Following the completion of each degradation step, electrochemical characterization was performed, including polarization curves and Electrochemical Impedance Spectroscopy (EIS) (stages from 1 to 3 in Table 2.2).

Based on the study by Wei et al.[18] a membrane regeneration procedure was performed at stage 4. This involved immersing the MEA in a 1M H_2SO_4 solution at 80°C for an hour. Subsequently, the membrane was rinsed with ultrapure water (Milli-Q®, 18.2 MΩ).

In order to conduct water analysis before and after degradations, samples were taken at the beginning of stage 0 and at the end of stage 2. The conductivity and concentration of titanium, fluoride, calcium, sodium and sulfate were measured in both samples.

3. Results and Discussion

3.1 Polarization curves, chronoamperometric and chronopotentiometric studies

Operation curve under experimental conditions is depicted in Figure 3.1 for pristine cell (pre degradation condition) and after degradation procedures.

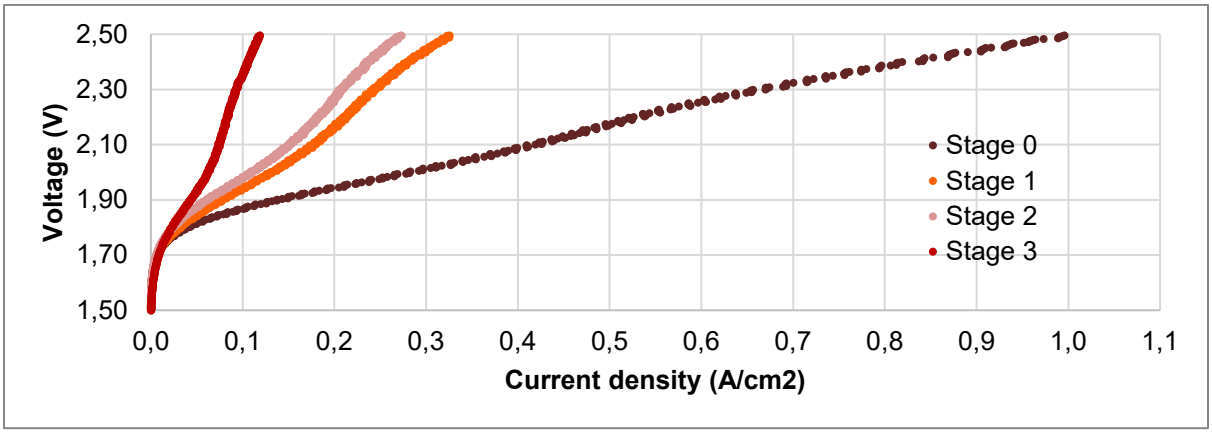

Figure 3.1 – Polarization curves of the cell at four different degradation stages. Initial conditions (stage 0), two successive steps of 168 h of constant voltage operation at 2V (stages 1 and 2) and a final galvanostatic step at 2.3 A (stage 3).

In the first two stages of the degradation test (stages 1 and 2 respectively, see Table 2.2), water electrolysis was run at a constant cell voltage mode (setting value 2V). Consequently, current density declines and thus, hydrogen production decrease was observed during the whole period of degradation, as shown in Figure 3.2.

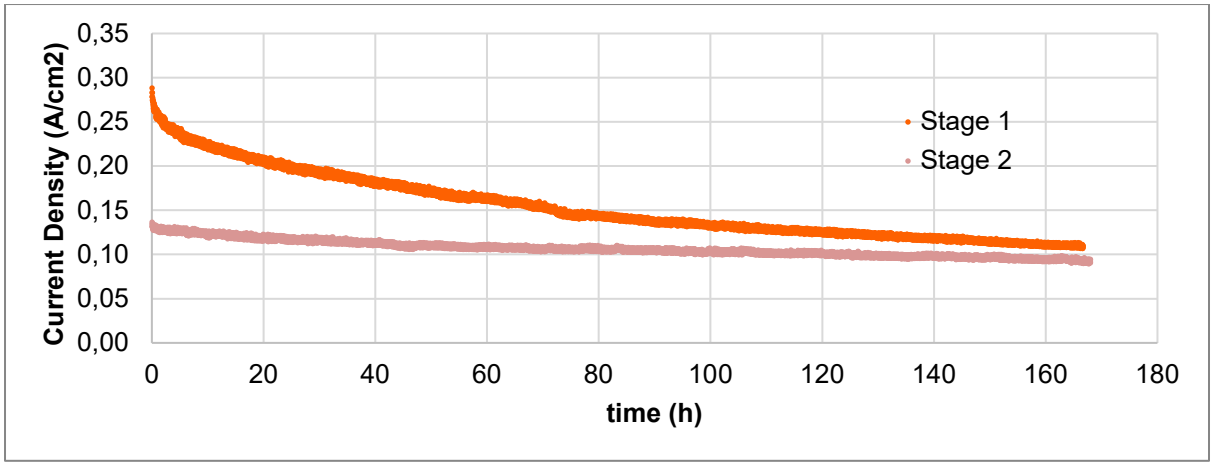

Figure 3.2 – Current density evolution (J) during constant operation over two steps of 168 h at 2V for Stage 1 and 2.

It is worthwhile noticing that current density during stage 1 decreases faster than during stage 2. Degradation rate values over time are shown in Figure 3.3.
After both periods degradation rates stabilize at values close to 250μA/h cm^2.

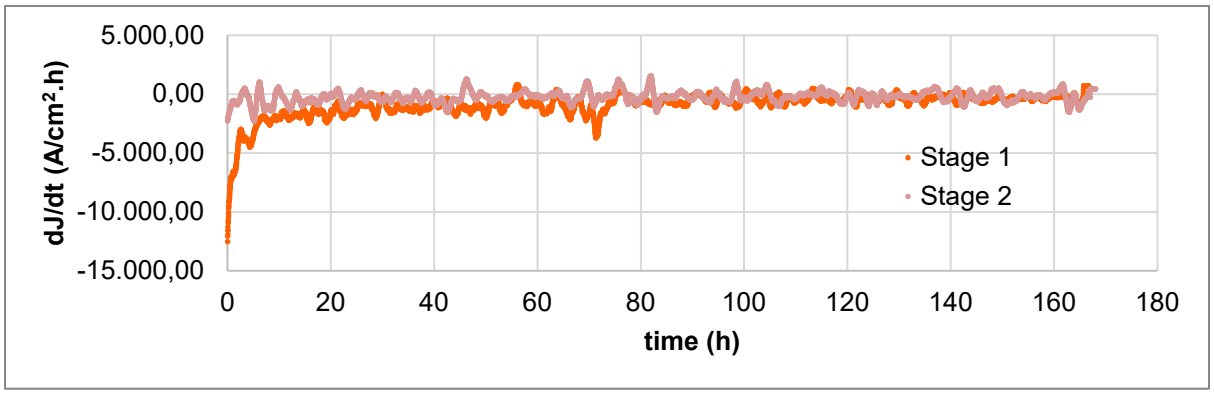

Figure 3.3 – Degradation rate during constant operation over two steps of 168 h at 2V for Stage 1 and 2.

After these two potentiostatic steps of degradation a galvanostatic degradation stage was carried out as shown in Figure 3.4.

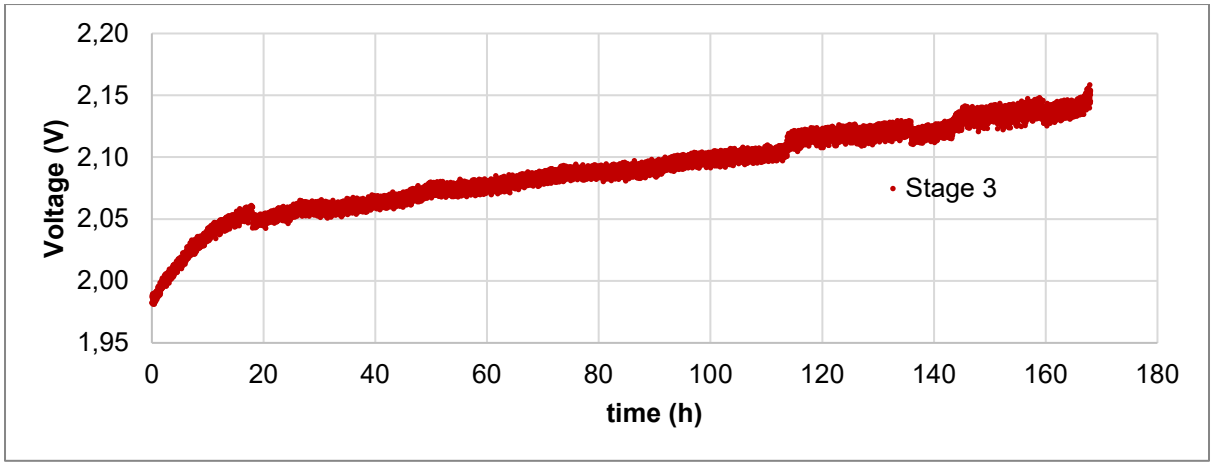

Figure 3.4 – Voltage evolution during constant operation over 168 h at 2.3 A for Stage 3.

Consequently, during this study, voltage value rises and thus an increase of electric power is required to maintain a constant current density as shown in Figure 3.5.

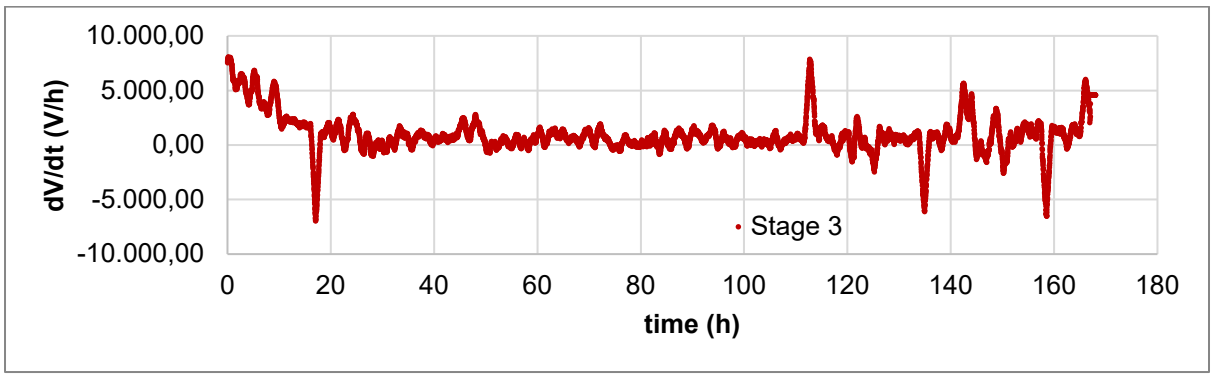

Figure 3.5 – Rate of change of voltage over time during constant operation over 168 h at 2.3 A for Stage 3.

Next, a regeneration procedure in acid media was carried out. Figure 3.6 shows operation curves after regeneration (stage 4) together with the previous state of the MEA (stage 3) and its initial condition (stage 0).

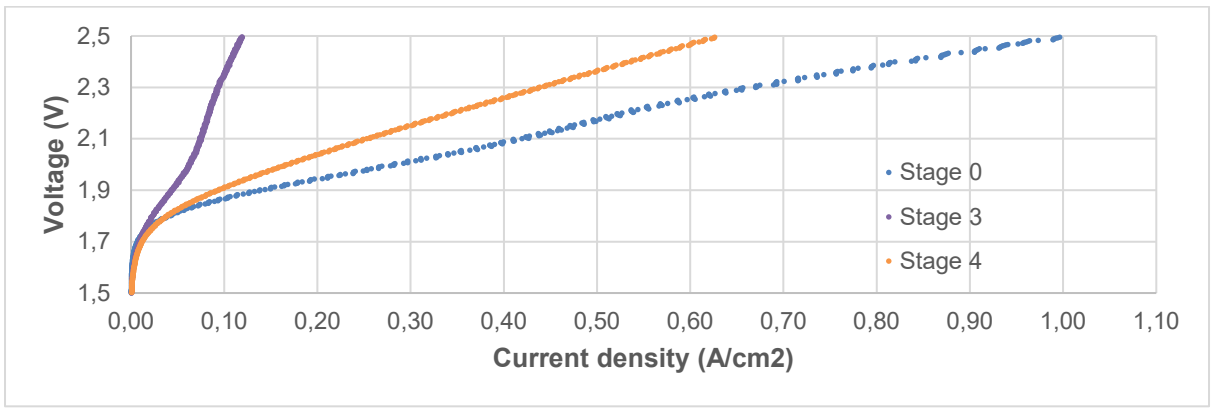

Figure 3.6 – Polarization curves of the cell at pristine conditions (Stage 0), after the first 3 stages of degradation (Stage 3) and after regeneration procedure (Stage 4).

To evaluate regeneration effects on degradation rate, another degradation step was carried out as can be seen in Figure 3.7. After acidic treatment the MEA partially restores its current performance with slower degradation rates of 40 μA/h cm^2 as shown in Figure 3.8, roughly six times slower than values reported before regeneration procedure.
During the sulfuric acid treatment for an hour to protonate the Nafion, contamination should be removed, indicating performance decline of the MEA is mainly produced by a reversible contamination.

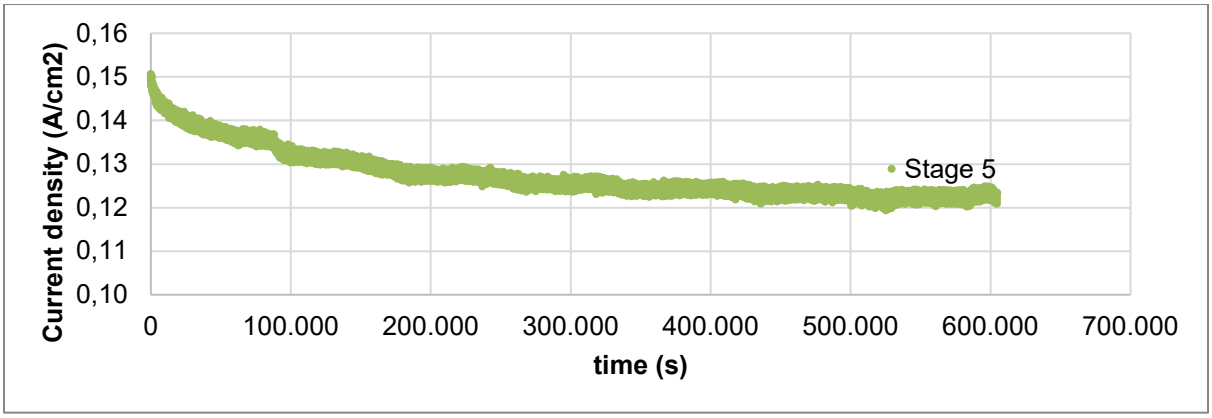

Figure 3.7 – Current density (J) evolution during constant operation at 2 V over 168 h after the regeneration procedure was carried out.

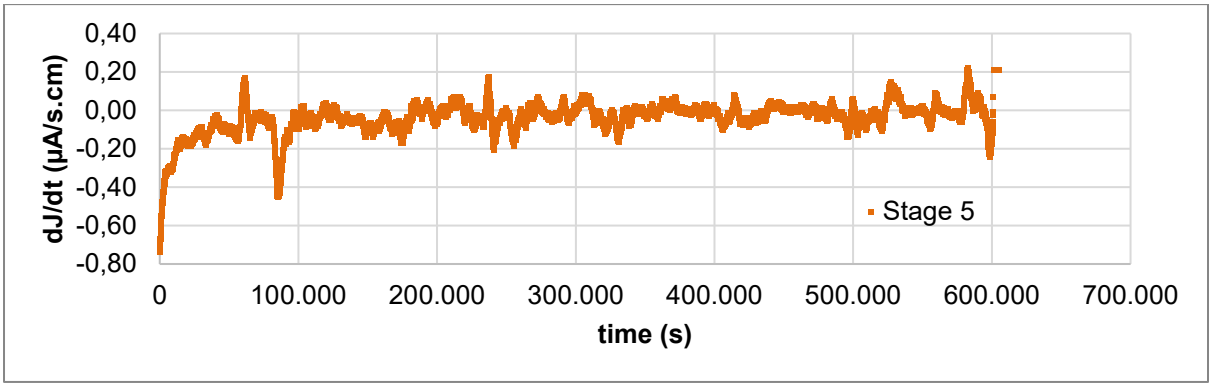

Figure 3.8 – Rate of change of current density over time during constant operation at 2V over 168 h after the regeneration procedure was carried out.

3.2 Electrochemical impedance spectroscopy

Figure 3.9 and Figure 3.10 depict Nyquist plots for studied configuration at 1.9 V and 2.3 V for 60°C respectively. The equivalent impedance of the cell was studied to isolate the different processes that occur inside the cell and their change during operation. 1.9 V (low current densities) and 2.3 V (higher current density) correspond to points on the polarization curve related to regions under activation control and mass transfer control, respectively.

At low current densities, when the impact of concentration overvoltage is disregarded, two series-connected RCPE branches can replicate the activation voltage drop of the anode and cathode compartments separately[19]. Apart from inductor and ohmic resistance element present at low and higher current densities. Inductive behaviour is not shown.

At higher current densities, the series-connected RCPE branches replicate the activation voltage drop and the effects of concentration overvoltage. This approach is widely accepted for modelling both galvanic and electrolytic cells[20]

The impedance parameters were obtained by fitting from the equivalent circuit model illustrated in Figure 2.3 where R_{Ω}, R_{cat}, and R_{an} represent the ohmic and charge transfer resistances (cathodic and anodic), while Y_{cat}, Y_{an}, a_{cat}, and a_{an} denote the pseudo capacitances and the exponents of the charge transfer constant phase elements. For 2.3V parameters derived for the second branch (R_m, Y_m and a_m) are related to diffusion process effects. The impedance of the constant phase elements (CPE) was calculated following the method outlined in Lasia [21].

To identify changes in the system, time constants were determined for each RCPE branch using the fitted parameters. τ_{cat}, τ_{an} and τ_m refer to the cathodic charge transfer time constant, anodic charge transfer time constant and diffusion time constant respectively. See Table 3.1 and Table 3.2.

Table 3.1 – Parameters fitted for measurements at 1.9 V

		1.9 V					
Parameter	Units	Stage 0	Stage 1	Stage 2	Stage 3	Stage 4	Stage 5
L_{stray}	H	2,26E-07	2,74E-07	2,73E-07	2,74E-07	1,53E-07	1,70E-07
R_{Ω}	ohm	1,23E-02	1,44E-02	1,49E-02	2,97E-02	2,81E-02	2,91E-02
R_{cat}	ohm	2,07E-03	1,18E-02	1,94E-02	4,84E-02	3,20E-03	1,42E-02
Y_{cat}	S.s^n1	3,95E+00	1,13E+00	9,28E-01	2,88E+00	3,14E+00	2,31E+00
a_{cat}		6,89E-01	7,12E-01	7,17E-01	4,20E-01	5,60E-01	5,30E-01
R_{an}	ohm	1,45E-02	2,99E-02	3,55E-02	5,07E-02	2,73E-02	3,32E-02
Y_{an}	S.s^n2	3,14E+00	2,43E+00	2,33E+00	2,43E+00	2,90E+00	2,60E+00
a_{an}		8,94E-01	8,49E-01	8,93E-01	8,59E-01	8,82E-01	8,56E-01
τ_{cat}	s	9,30E-04	2,30E-03	3,68E-03	9,20E-03	2,69E-04	1,58E-03
τ_{an}	s	3,17E-02	4,55E-02	6,13E-02	8,75E-02	5,63E-02	5,72E-02
χ^2	ohm	3,55E-03	1,45E-02	6,76E-03	1,04E-03	4,41E-04	8,12E-04

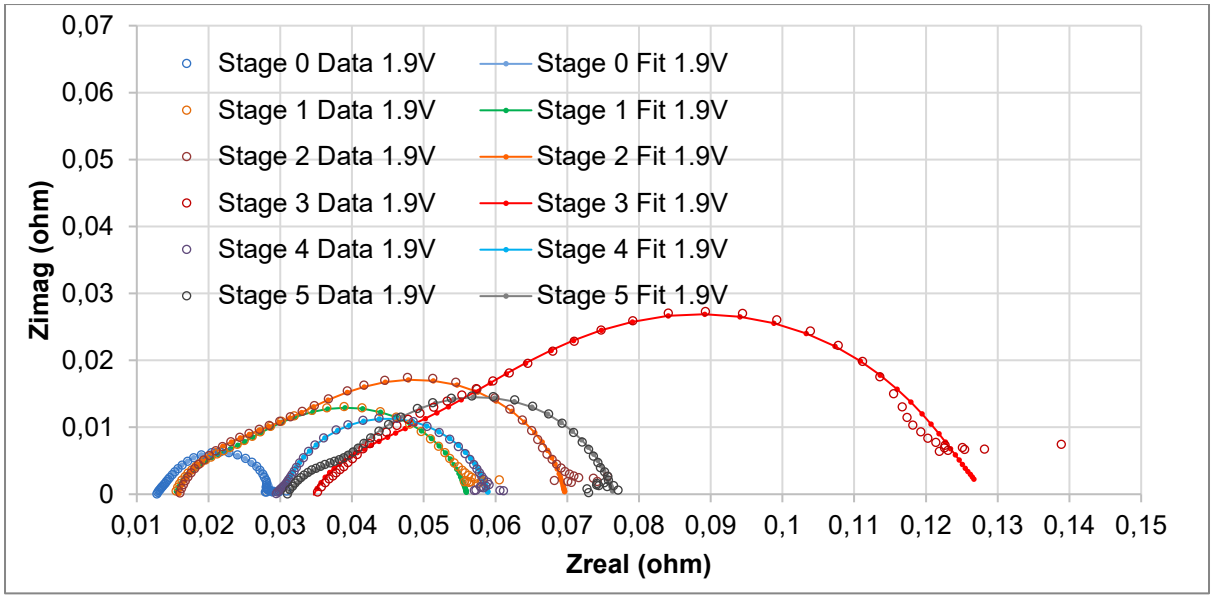

Figure 3.9 – Nyquist plot fitted at 1.9 V.

Table 3.2 – Parameters fitted for measurements at 2.3 V

		2.3 V					
Parameter	Units	Stage 0	Stage 1	Stage 2	Stage 3	Stage 4	Stage 5
L	H	1,83E-07	2,71E-07	2,66E-07	7,58E-08	1,31E-07	1,64E-07
R_Ω	ohm	1,23E-02	1,52E-02	1,63E-02	3,68E-02	2,85E-02	2,96E-02
R_{an}	ohm	3,40E-03	1,91E-02	2,96E-02	8,60E-02	1,86E-03	5,93E-03
Y_{an}	S.s^n1	3,45E+00	2,49E+00	2,58E+00	1,68E+00	1,43E+00	3,40E-01
a_{an}		8,39E-01	7,04E-01	6,67E-01	6,52E-01	7,49E-01	7,88E-01
R_m	ohm	3,55E-02	1,82E-01	2,57E-01	6,26E-01	3,51E-03	7,37E-03
Y_m	S.s^n2	7,52E+01	2,23E+01	2,54E+01	1,90E+01	3,98E+00	3,52E+00
a_m		3,12E-01	4,56E-01	4,74E-01	5,81E-01	8,61E-01	8,12E-01
τ_{an}	s	4,98E-03	1,33E-02	2,11E-02	5,14E-02	3,65E-04	3,79E-04
τ_m	s	2,33E+01	2,18E+01	5,23E+01	7,11E+01	7,01E-03	1,11E-02
χ^2	ohm	8,60E-04	4,71E-03	2,46E-03	1,17E-02	7,23E-02	8,57E-02

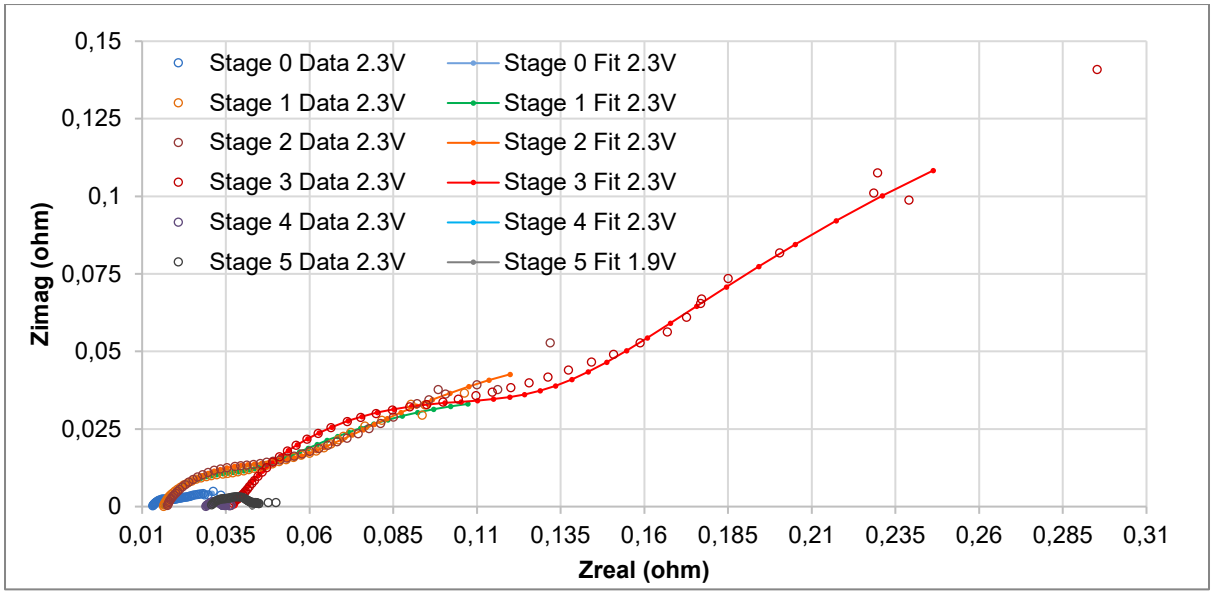

Figure 3.10 – Nyquist plot fitted at 2.3 V.

Each Nyquist plot depicted different regions which correspond to the frequency range in the impedance spectrum. Plots show an inductive structure at high frequencies where L is an inductor introduced by the current collector (not shown), R_Ω explains the voltage drop due to the current collectors and the resistance due to the lack of contact between the binder, the electrode particles, and the electrolyte. Besides, Nyquist plots depict two depressed semi-circles associated with faradaic and mass transfer processes. Results of fitted parameters are depicted in Table 3.2.

Figure 3.11, Figure 3.12, Figure 3.13, Figure 3.14 show the evolution of parameters during degradation of R_Ω, τ_{cat}, τ_{an} and τ_m respectively

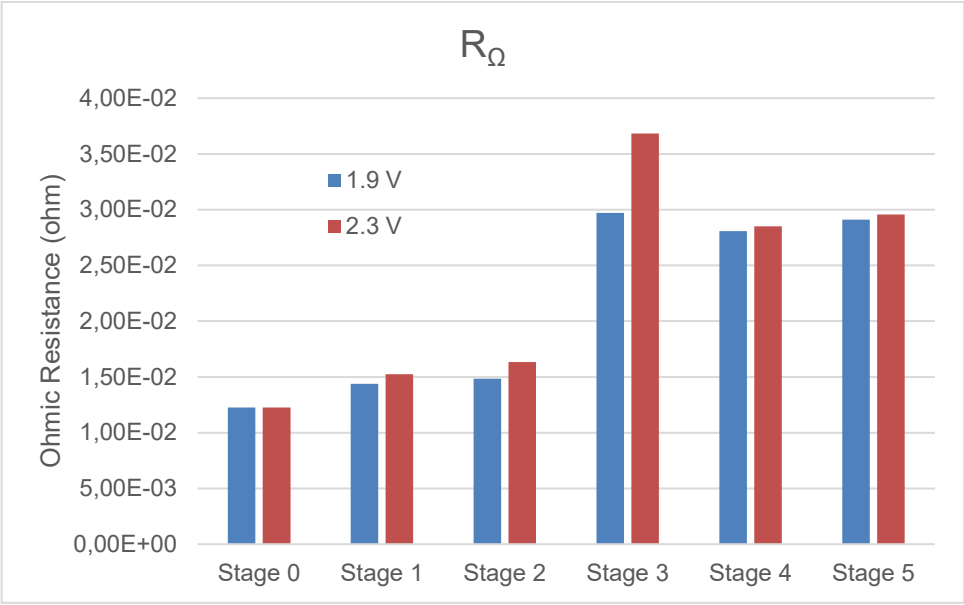

Figure 3.11 – Ohmic resistance for each stage at 1.9V and 2.3V.

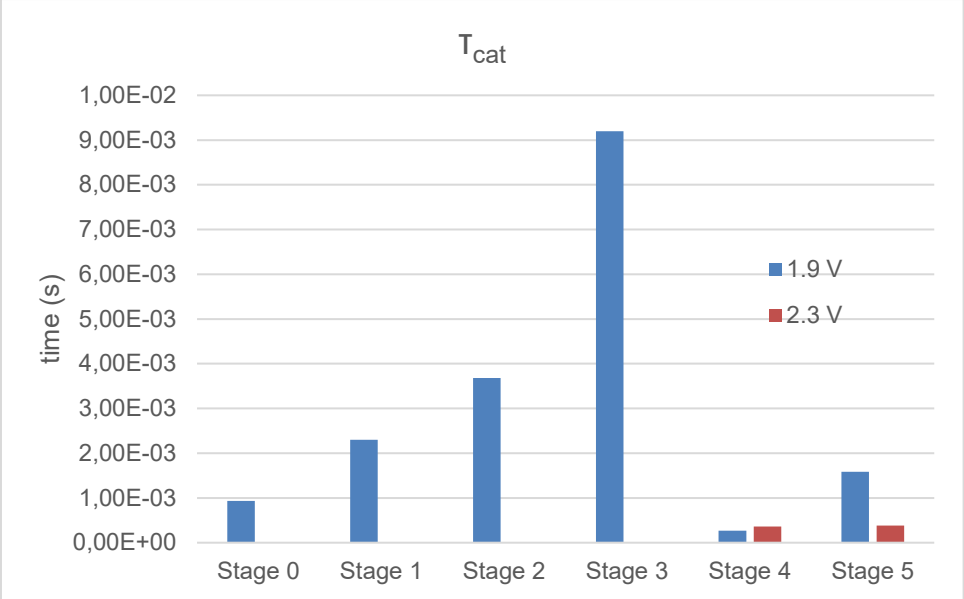

Figure 3.12 – Time constant for cathodic charge transfer for each stage at 1.9V and 2.3V.

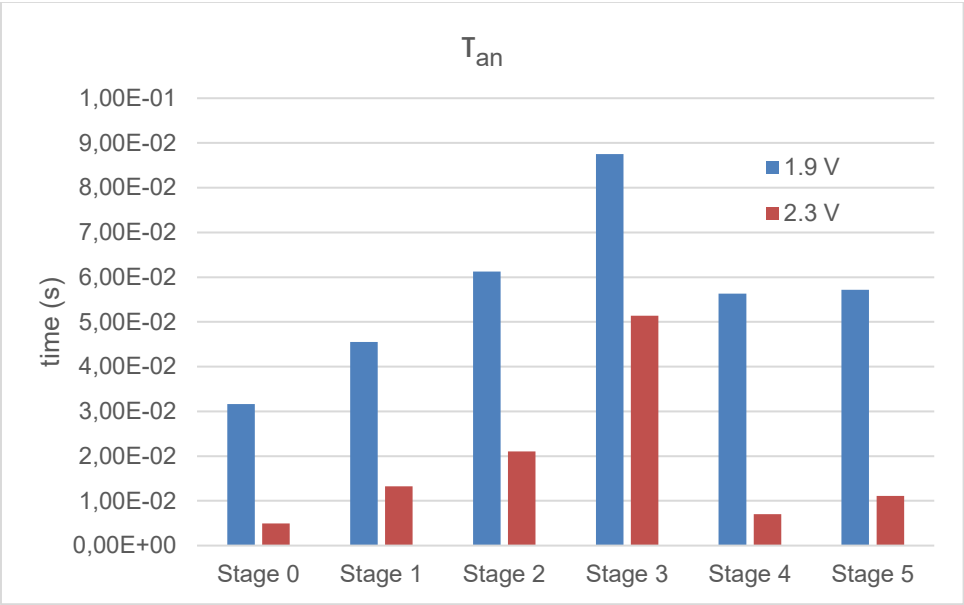

Figure 3.13 – Time constant for anodic charge transfer for each stage at 1.9V and 2.3V.

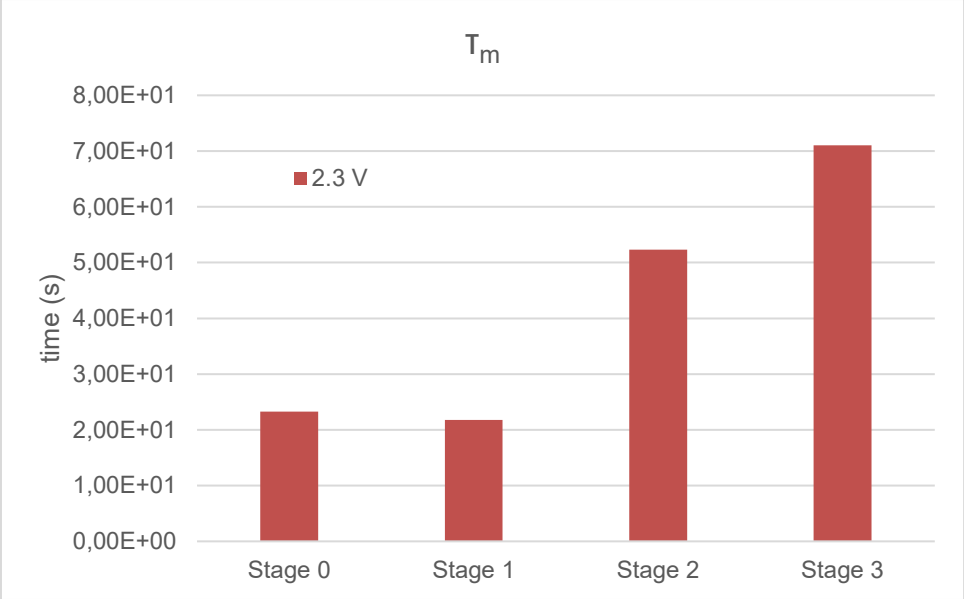

Figure 3.14 – Time constant for mass transfer for each stage at 1.9V and 2.3V.

Ohmic resistance presents a significant increase after degradation 3 (galvanostatic step) and does not recover after regeneration.

For 1.9V (where charge transfer control is detected) it is observed that the anodic and cathodic time constants increase during degradation. After regeneration, a significance decrease of this value is depicted. It should be noted that this effect is more marked in the cathodic time constant (compatible with the removal of reduced impurities).

For 2.3V (where mass transfer control is observed) the time constant associated with faradaic processes increases during degradation and decreases significantly because of regeneration.

During degradation, mass transfer time constant also shows an increase in its value.

Regarding the water analysis, fluoride was the only analyte with a noticeable concentration increase between the initial and measured stage. According to UNE EN ISO10304-1:2009 analysis, the initial fluoride concentration value was lower than the detection limit and after the degradation the determined value was 1.5 $mg.L^{-1}$. It is worthwhile noticing that this increase should be associated with membrane degradation (irreversible deterioration)

4. Conclusions

The degradation of the assembly under different working conditions is evaluated using electrochemical techniques.

After acidic treatment the MEA partially restores its original performance with slower degradation rates of 40 $\mu A/h\ cm^2$, six times slower than values reported before regeneration study.

Performance decline of the MEA is mainly produced by a reversible contamination, time constant reach values like pristine assembly. The higher degradation rate observed in Stage 1 could be associated with the blocking of most active sites as a result of the reduction of impurities on the surface of the electrocatalyst, as well as the clogging of membrane pores. In the subsequent stages of degradation, there is an increase in the thickness of these deposits, primarily affecting the resistance.

However, a irreversible deterioration is observed evidenced by the increase in ohmic resistance that does not decrease after regeneration. This irreversible deterioration would be associated with the degradation of the Nafion membrane.
The water samples taken at the end of the experiment show the presence of fluorides, which could be due to several factors that might contribute to the deterioration of the membrane. These factors include chemical attack by oxidizing agents (e.g hydrogen peroxide) present during operation, mechanical wear caused by repeated stresses on the membrane, thermal degradation due to operating temperatures, and electrode contamination. These mechanisms would create conditions that facilitate degradation processes and, consequently, the release of fluorides into the water.

Acknowledgments

The authors appreciate the support from CSIC-UdelaR, PEDECIBA and ANII, E.T., and V.D. are researchers at PEDECIBA/United Nations.

References

(1) Shiva Kumar, S.; Himabindu, V. Hydrogen Production by PEM Water Electrolysis – A Review. *Mater. Sci. Energy Technol.* **2019**, *2* (3), 442–454. https://doi.org/10.1016/j.mset.2019.03.002.

(2) Pivovar, B.; Rustagi, N.; Satyapal, S. Hydrogen at Scale (H_2 @Scale): Key to a Clean, Economic, and Sustainable Energy System. *Electrochem. Soc. Interface* **2018**, *27* (1), 47–52. https://doi.org/10.1149/2.F04181if.

(3) Grigoriev, S. A.; Dzhus, K. A.; Bessarabov, D. G.; Millet, P. Failure of PEM Water Electrolysis Cells: Case Study Involving Anode Dissolution and Membrane Thinning. *Int. J. Hydrog. Energy* **2014**, *39* (35), 20440–20446. https://doi.org/10.1016/j.ijhydene.2014.05.043.

(4) Cherevko, S.; Reier, T.; Zeradjanin, A. R.; Pawolek, Z.; Strasser, P.; Mayrhofer, K. J. J. Stability of Nanostructured Iridium Oxide Electrocatalysts during Oxygen Evolution Reaction in Acidic Environment. *Electrochem. Commun.* **2014**, *48*, 81–85. https://doi.org/10.1016/j.elecom.2014.08.027.

(5) Chandesris, M.; Médeau, V.; Guillet, N.; Chelghoum, S.; Thoby, D.; Fouda-Onana, F. Membrane Degradation in PEM Water Electrolyzer: Numerical Modeling and Experimental Evidence of the Influence of Temperature and Current Density. *Int. J. Hydrog. Energy* **2015**, *40* (3), 1353–1366. https://doi.org/10.1016/j.ijhydene.2014.11.111.

(6) Albert, A.; Lochner, T.; Schmidt, T. J.; Gubler, L. Stability and Degradation Mechanisms of Radiation-Grafted Polymer Electrolyte Membranes for Water Electrolysis. *ACS Appl. Mater. Interfaces* **2016**, *8* (24), 15297–15306. https://doi.org/10.1021/acsami.6b03050.

(7) Feng, Q.; Yuan, X.; Liu, G.; Wei, B.; Zhang, Z.; Li, H.; Wang, H. A Review of Proton Exchange Membrane Water Electrolysis on Degradation Mechanisms and Mitigation Strategies. *J. Power Sources* **2017**, *366*, 33–55. https://doi.org/10.1016/j.jpowsour.2017.09.006.

(8) Jung, H.-Y.; Huang, S.-Y.; Ganesan, P.; Popov, B. N. Performance of Gold-Coated Titanium Bipolar Plates in Unitized Regenerative Fuel Cell Operation. *J. Power Sources* **2009**, *194* (2), 972–975. https://doi.org/10.1016/j.jpowsour.2009.06.030.

(9) Gago, A. S.; Ansar, S. A.; Saruhan, B.; Schulz, U.; Lettenmeier, P.; Cañas, N. A.; Gazdzicki, P.; Morawietz, T.; Hiesgen, R.; Arnold, J.; Friedrich, K. A. Protective Coatings on Stainless Steel Bipolar Plates for Proton Exchange Membrane (PEM) Electrolysers. *J. Power Sources* **2016**, *307*, 815–825. https://doi.org/10.1016/j.jpowsour.2015.12.071.

(10) Majasan, J. O.; Iacoviello, F.; Shearing, P. R.; Brett, D. J. Effect of Microstructure of Porous Transport Layer on Performance in Polymer Electrolyte Membrane Water Electrolyser. *Energy Procedia* **2018**, *151*, 111–119. https://doi.org/10.1016/j.egypro.2018.09.035.

(11) Mo, J.; Kang, Z.; Yang, G.; Retterer, S. T.; Cullen, D. A.; Toops, T. J.; Green, J. B.; Zhang, F.-Y. Thin Liquid/Gas Diffusion Layers for High-Efficiency Hydrogen Production from Water Splitting. *Appl. Energy* **2016**, *177*, 817–822. https://doi.org/10.1016/j.apenergy.2016.05.154.

(12) Hoeh, M. A.; Arlt, T.; Kardjilov, N.; Manke, I.; Banhart, J.; Fritz, D. L.; Ehlert, J.; Lüke, W.; Lehnert, W. In-Operando Neutron Radiography Studies of Polymer Electrolyte Membrane Water Electrolyzers. *ECS Trans.* **2015**, *69* (17), 1135–1140. https://doi.org/10.1149/06917.1135ecst.

(13) Mo, J.; Steen, S. M.; Zhang, F.-Y.; Toops, T. J.; Brady, M. P.; Green, J. B. Electrochemical Investigation of Stainless Steel Corrosion in a Proton Exchange Membrane Electrolyzer Cell. *Int. J. Hydrog. Energy* **2015**, *40* (36), 12506–12511. https://doi.org/10.1016/j.ijhydene.2015.07.061.

(14) Mo, J.; Dehoff, R. R.; Peter, W. H.; Toops, T. J.; Green, J. B.; Zhang, F.-Y. Additive Manufacturing of Liquid/Gas Diffusion Layers for Low-Cost and High-Efficiency Hydrogen Production. *Int. J. Hydrog. Energy* **2016**, *41* (4), 3128–3135. https://doi.org/10.1016/j.ijhydene.2015.12.111.

(15) Lee, C.; Hinebaugh, J.; Banerjee, R.; Chevalier, S.; Abouatallah, R.; Wang, R.; Bazylak, A. Influence of Limiting Throat and Flow Regime on Oxygen Bubble Saturation of Polymer Electrolyte Membrane Electrolyzer Porous Transport Layers. *Int. J. Hydrog. Energy* **2017**, *42* (5), 2724–2735. https://doi.org/10.1016/j.ijhydene.2016.09.114.

(16) Tomić, A. Z.; Pivac, I.; Barbir, F. A Review of Testing Procedures for Proton Exchange Membrane Electrolyzer Degradation. *J. Power Sources* **2023**, *557*, 232569. https://doi.org/10.1016/j.jpowsour.2022.232569.
(17) Rojas Tattá, R.; Teliz, E.; Díaz, V. Spectroscopy Electrochemical Impedance Characterization of Membranes Electrode Assemblies for PEM Electrolyzers. *Int. J. Chem. React. Eng.* **2024**, *22* (2), 97–109. https://doi.org/10.1515/ijcre-2023-0134.
(18) Wei, G.; Wang, Y.; Huang, C.; Gao, Q.; Wang, Z.; Xu, L. The Stability of MEA in SPE Water Electrolysis for Hydrogen Production. *Int. J. Hydrog. Energy* **2010**, *35* (9), 3951–3957. https://doi.org/10.1016/j.ijhydene.2010.01.153.
(19) Khalid Ratib, M.; M. Muttaqi, K.; Islam, M. R.; Sutanto, D.; Agalgaonkar, A. P. Electrical Circuit Modeling of Proton Exchange Membrane Electrolyzer: The State-of-the-Art, Current Challenges, and Recommendations. *Int. J. Hydrog. Energy* **2024**, *49*, 625–645. https://doi.org/10.1016/j.ijhydene.2023.08.319.
(20) Martinson, C. A.; Van Schoor, G.; Uren, K. R.; Bessarabov, D. Characterisation of a PEM Electrolyser Using the Current Interrupt Method. *Int. J. Hydrog. Energy* **2014**, *39* (36), 20865–20878. https://doi.org/10.1016/j.ijhydene.2014.09.153.
(21) Lasia, A. *Electrochemical Impedance Spectroscopy and Its Applications*; Springer New York: New York, NY, 2014. https://doi.org/10.1007/978-1-4614-8933-7.
(22) Lazanas, A. Ch.; Prodromidis, M. I. Electrochemical Impedance Spectroscopy—A Tutorial. *ACS Meas. Sci. Au* **2023**, *3* (3), 162–193. https://doi.org/10.1021/acsmeasuresciau.2c00070.